rated with a minimal amount of pentane/benzene and filtered to give 0.78 g of yellow $Ta(\eta^5\text{-}C_5Me_5)(CHPh)(CH{=}PPh_3)Cl$ (64%). It can be recrystallized from toluene/pentane mixtures. Heptane (110 mg, 1.11 mmol) was added to the volatiles from the reaction, and toluene (1.21 mmol, 0.71 mmol/mmol of tantalum) was measured by GLC.

Anal. Calcd for $TaC_{36}H_{37}ClP$: C, 60.29; H, 5.21; P, 4.32. Found: C, 60.24; H, 5.43; P, 4.42. $^1H$ NMR ($C_6D_6$): $\tau$ 7.87 (s, 15, Me), 5.13 (dd, 1, $^2J_{HP}$ = 23 Hz, $^4J_{HH}$ = 2 Hz, C*H*=P), 3.39 (d, 1, $^4J_{HP}$ = 8 Hz, coupling to C*H*=P unresolved, =C*H*Ph), 2.78-3.15 and 2.15-2.38 (m, 20, $PPh_3$ and Ph). $^{13}C$ NMR ($C_6D_6$): $\delta$ 12.1 (q, $^1J_{CH}$ = 127 Hz, Me), 114.1 (s, $C_5Me_5$), 121.4-134.7 (complex, contains correct number of resonances for $PPh_3$, Ph, and *C*H=P carbons), 149.9 (s, $C_\beta$ in =CHPh), 206.6 (d, $^1J_{CH_\alpha}$ = 85 Hz, =*C*HPh).

**Acknowledgment.** We thank the National Science Foundation for support (Grant CHE76 07410 to R.R.S. and Grant CHE77 24964 to G.D.S.) and the Francis Bitter National Magnet Laboratory for use of their high-field NMR facilities.

# Photoelectron Study of the Interaction of CO with ZnO[1]

**Robert R. Gay, Mark H. Nodine, Victor E. Henrich, H. J. Zeiger, and Edward I. Solomon***

*Contribution from the Department of Chemistry, Massachusetts Institute of Technology, Cambridge, Massachusetts 02139, and Lincoln Laboratory, Massachusetts Institute of Technology, Lexington, Massachusetts 02173.* *Received November 9, 1979*

**Abstract:** Ultraviolet photoelectron spectroscopy (UPS) has been used to study the chemisorption of CO on four low-index surfaces of ZnO, an active methanol catalyst. These surfaces have significant differences with respect to their coordination unsaturation; thus, a correlation between the adsorption behavior and the surface structure enables the geometric requirements for chemisorption to be determined. The He II photoelectron peak associated with the $4\sigma$ molecular orbital of the CO molecule serves as a probe of the amount of adsorbed CO. The adsorption is found to be reversible, and measurements of the equilibrium coverage as a function of temperature and pressure demonstrate that the bonding interactions are very similar on all four surfaces, with an initial heat of adsorption of 12.0 ± 0.4 kcal/mol, which decreases approximately linearly with coverage. Chemisorbed CO is readily displaced by $NH_3$, indicating the involvement of zinc ions in the bonding of CO to the surface. This is strongly supported by the relative CO coverage of the four surfaces under equivalent conditions, which generally correlates with the availability of unsaturated zinc sites. Angle-resolved measurements of the $4\sigma$ intensity are used to confirm this binding mode. The bonding of CO to ZnO is dominated by the $\sigma$ donor interaction of the carbon end of the molecule with the zinc ion as determined from the observed decrease in the splitting of the energies of the $4\sigma$ and $5\sigma$ molecular orbitals. The lack of significant $\pi$ back-bonding is supported by the increase of the dipole moment of the coordinated CO molecule to ~0.6 D as determined from He I photoelectron work function measurements. This mode of binding of CO is consistent with the observed increase in the CO stretching frequency relative to the gas-phase value and suggests possible relevance to catalysis.

## Introduction

Studies of the interactions between CO and a variety of materials have been spurred by an interest in the electronic structure of CO complexes as well as in the reactivity of coordinated CO, since CO is the basic feedstock in a number of catalytic processes. While the interaction of CO with metals is currently the subject of intense study, the metal oxides are also extremely relevant as heterogeneous catalysts,[2] and their interactions with CO are somewhat unusual compared to those of known inorganic complexes.

One important system in which CO interacts with a metal oxide catalyst is the methanol synthesis reaction[3] (1). The earlier

$$CO + 2H_2 \xrightarrow[\substack{200\ atm\\400\ C}]{ZnO\text{-}CrO_3} CH_3OH \qquad (1)$$

industrial catalysts employed a mixture of zinc and chromium oxides, where it is believed that the active component in the catalyst is ZnO, which is prevented from sintering by the formation of a zinc chromite spinel, acting as an intercrystalline promoter.[4,5] Newer low-temperature, low-pressure Cu-Zn-Cr oxide catalyst mixtures have been developed,[6,7] in which the active material has been suggested to be Cu substituted for Zn in ZnO surface sites.[8] The mechanism of the reaction has not been clarified for any of these catalysts. A number of reaction intermediates have been proposed and a variety of "rate-determining" steps have been suggested.[9-21] In particular, there has been much speculation

* Massachusetts Institute of Technology, Cambridge, Mass.

(1) This material has been presented at: (a) Gay, R. R.; Solomon, E. I.; Henrich, V. E.; Zeiger, H. J. 174th National Meeting of the American Chemical Society, Anaheim, CA, 1978; (b) Gay, R. R.; Solomon, E. I.; Henrich, V. E.; Zeiger, H. J. Thirty-Eighth Annual Conference on Physical Electronics, Oak Ridge, TN, 1978; (c) Gay, R. R.; Solomon, E. I.; Henrich, V. E.; Zeiger, H. J. 175th National Meeting of the American Chemical Society, Honolulu, HI, 1979, (d) Gay, R. R.; Solomon, E. I.; Henrich, V. E.; Zeiger, H. J. Thirty-Ninth Annual Conference on Physical Electronics, College Park, MD, 1979.

(2) Krylov, O. V. "Catalysis by Nonmetals"; Academic Press: New York, 1970.

(3) Waddams, A. L. "Chemicals from Petroleum", 3rd ed.; Wiley: New York, 1973.

(4) Emmett, P. H. In "Catalysis Then and Now"; Emmet, P. H.; Sabatier, P.; Reid, E. E., Eds.; Franklin Publishing Co., Inc.: Englewood, NJ, 1965; Part I, p 173-186.

(5) Burzyk, J.; Haber, J. *Bull. Acad. Pol. Sci., Ser. Sci. Chim.* **1969**, *17*, 531, 539. Burzyk, J.; Haber, J.; Nowotny, J. *Ibid.* **1969**, *17*, 543.

(6) Imperial Chemical Industries Ltd.; Methanol Catalyst.

(7) Mehta, D. D.; Ross, D. E. *Hydrocarbon Process.* **1970**, *183*.

(8) Klier, K.; Simmons, G. W.; Herman, R. G.; Mehta, S. "Winter Newsletter - January 1979", Division of Inorganic Chemistry, American Chemical Society; ACS/CSJ Chemical Congress: Honolulu, Hawaii, April 2-6, 1979; No. 315.

(9) Nagarjunan, T. S.; Sastri, M. V. C.; Kuriacose, T. *J. Catal.* **1963**, *2*, 223.

(10) Tsuchiya, S.; Shiba, T. *J. Catal.* **1965**, *4*, 116.

(11) Tsuchiya, S.; Shiba, T. *Bull. Chem. Soc. Jpn.* **1965**, *38*, 1726.

(12) Tsuchiya, S.; Shiba, T. *Bull. Chem. Soc. Jpn.* **1967**, *40*, 1086.

(13) Tsuchiya, S.; Shiba, T. *Bull. Chem. Soc. Jpn.* **1968**, *41*, 573.

(14) Uchida, H.; Oba, M.; Isogai, N.; Hasegawa, T. *Bull. Chem. Soc. Jpn.* **1968**, *41*, 497.

(15) Borowitz, J. L. *J. Catal.* **1969**, *13*, 106.

(16) Aharoni, C.; Tompkins, F. C. *Trans. Faraday Soc.* **1970**, *66*, 434.

(17) Ueno, A.; Onishi, T.; Tamaru, K. *Trans. Faraday Soc.* **1971**, *67*, 3585.

0002-7863/80/1502-6752$01.00/0 

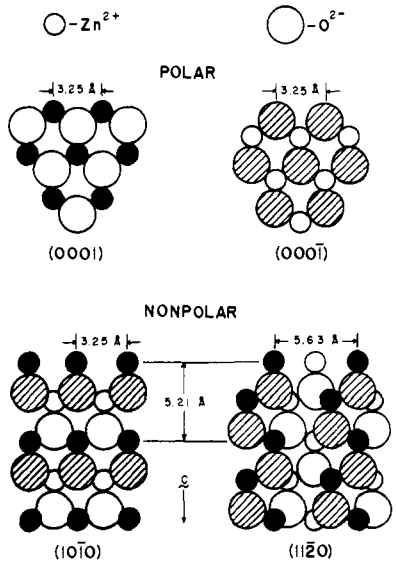


**Figure 1.** Surface geometry of the four low-index surfaces of ZnO. Large circles represent oxide ions, small circles represent zinc ions, shaded circles represent the surface layer, and open circles represent the second layer. Dimensions have been taken from ref 26.

concerning the geometric and electronic structure of the complex formed by coordination of CO to sites on the zinc oxide surface.

Measurements of the interaction of CO with ZnO powders by infrared spectroscopy have shown that the CO stretching frequency *increases* upon adsorption[19,20,22] contrary to its general behavior for organometallic compounds. For those organometallic compounds where the stretching frequency does increase,[23] one model that has been suggested involves an oxygen-bound, M–OC species.[24] An alternative model simply invokes the variation in the extent of $\sigma$ donation and $\pi$ back-bonding between the metal and the CO molecule.[25] For ZnO, a third view that CO binds dominantly to the surface oxides has also been recently emphasized.[27]

In order to determine the geometric and electronic structure of CO adsorbed on ZnO, we have chosen to study the interaction of CO with clean, well-defined, single-crystal ZnO surfaces. The wurtzite structure of ZnO provides a large variation of low-index surface geometries, as shown in Figure 1. Ideally, the (0001) surface may be viewed as a plane of zinc(II) ions with their coordinatively unsaturated bonds normal to the surface. The (000$\bar{1}$) surface would have the same structure, with the interchange of oxide ($O^{2-}$) ions and zinc ions. As these surfaces are composed of only one type of ion, they are referred to as "polar" faces. The (10$\bar{1}$0) and (11$\bar{2}$0) surfaces are composed of equal numbers of zinc and oxide ions and are referred to as "nonpolar" faces. On the (10$\bar{1}$0) face, the zinc and oxide ions are arranged in pairs in the surface plane, while on the (11$\bar{2}$0) face they are arranged in chains. The directions of the coordinatively unsaturated bonds are tilted from the surface normal but at different angles on the two nonpolar surfaces.

Although no reconstruction occurs on the basis of the symmetry of the low-energy electron diffraction (LEED) pattern, small deviations from the bulk structure for these surfaces have been determined by dynamic analysis of the intensity vs. voltage profiles from LEED measurements.[28-44] For the (0001) surface, the zinc ions relax into the threefold site described by the coordinated oxide ions by about 0.3 Å. On the (10$\bar{1}$0) surface, the zinc ions relax into the surface about 0.45 Å and laterally by about 0.1 Å, with only a slight (<0.1 Å) variation in the oxide ion positions. The (000$\bar{1}$) and (11$\bar{2}$0) surfaces have been reported to retain the bulk structure. A second refinement to the above picture, inferred from streaking in the LEED patterns, is that both polar faces are stepped,[45-49] with a step height of one unit cell (two double layers) along the *c*-axis, in the {10$\bar{1}$0} directions, exposing nonpolar faces.

It was anticipated that the geometric requirements for chemisorption could be determined by studying the variation in adsorption behavior as a function of surface geometry. Surface-sensitive electron spectroscopic techniques were used to study the adsorption. As electron beams were found either to decompose or to displace adsorbed CO, photons were used as an excitation source. Since most of the information concerning the electronic changes brought about by chemisorption is found in the valence band structure of both the ZnO and the adsorbed CO molecules, the technique of ultraviolet photoelectron spectroscopy (UPS) was chosen. The He II line (40.8 eV) was primarily used since it enabled the measurement of binding energies as deep as 20 eV below the Fermi level while maintaining a high cross section for valence band photoionization and a low inelastically scattered background intensity. The He I photoelectron spectra were also studied since the onset of the photoelectric effect from the inelastic electron tail provides a direct measure of the change in the work function upon adsorption, leading to the dipole moment of the CO adsorption complex.

In this paper we report UPS studies of CO chemisorption on the (0001), (000$\bar{1}$), (10$\bar{1}$0), and (11$\bar{2}$0) faces of ZnO. The CO chemisorption is found to be dependent upon temperature, pressure, and, most importantly, the crystal face. The He II UPS spectrum and its angular dependence, competition experiments with ammonia, and the He I UPS work function measurements as a function of coverage ($\theta$) allow a specific geometric and electronic structural model of the active site for the chemisorption of CO on ZnO to be formulated.

## Experimental Section

All measurements were made in an ion-pumped ultrahigh vacuum (UHV) system. Base pressure after bakeout was $<5 \times 10^{-10}$ torr. The system was equipped with a Physical Electronics double-pass cylindrical

(18) Aharoni, C.; Starer, H. *Can. J. Chem.* **1974**, *52*, 4044.
(19) Voroshilov, I. G.; Roev, L. M.; Kozub, G. M.; Lunev, N. K.; Pavloskii, N. A.; Rusov, M. T. *Theor. Exp. Chem. (Engl. Transl.)* **1975**, *11*, 212.
(20) Boccuzzi, F.; Garrone, E.; Zecchina, A.; Bossi, A.; Camia, M. *J. Catal.* **1978**, *51*, 160.
(21) Carnisio, G.; Garbassi, F.; Petrini, G.; Parravano, G. *J. Catal.* **1978**, *54*, 66.
(22) Hush, N. S.; Williams, M. L. *J. Mol. Spectrosc.* **1974**, *50*, 349.
(23) Wender, I., Pino, P., Eds. "Organic Synthesis via Metal Carbonyls"; Wiley-Interscience: New York, 1968; Vol. 1, p 221.
(24) Nyholm, R. S. *Proc. Chem. Soc., London* **1961**, 273.
(25) Huber, H.; Ozin, G. A. *Inorg. Chem.* **1977**, *16*, 64.
(26) Abrahams, S. C.; Bernstein, J. L. *Acta Crystallogr., Sect. B* **1969**, *B25*, 1233.
(27) Lüth, H.; Rubloff, G. W.; Grobman, W. D. *Solid State Commun.* **1976**, *18*, 1427.
(28) Müller, K. In "The Structure and Chemistry of Solid Surfaces"; Somorjai, G. A., Ed.; Wiley: New York, 1969; p 35.
(29) Chung, M. F.; Farnsworth, H. E. *Surf. Sci.* **1970**, *22*, 93.
(30) Levine, J. D.; Willis, A.; Bottoms, W. R.; Mark, P. *Surf. Sci.* **1972**, *29*, 144.
(31) van Hove, H.; Leysen, R. *Phys. Status Solidi A* **1972**, *9*, 361.
(32) Fiermans, L.; Arijs, E.; Vennik, J.; Maenhout-van der Vorst, W. *Surf. Sci.* **1973**, *39*, 357.
(33) Leysen, R.; van Orshaegen, G.; van Hove, H.; Neyens, A. *Phys. Status Solidi A* **1973**, *18*, 613.
(34) Chang, S. C.; Mark, P. *Surf. Sci.* **1974**, *45*, 721.
(35) Chang, S. C.; Mark, P. *Surf. Sci.* **1974**, *46*, 293.
(36) Hopkins, B. J.; Leysen, R.; Taylor, P. A. *Surf. Sci.* **1975**, *48*, 486.
(37) Duke, C. B.; Lubinsky, A. R. *Surf. Sci.* **1975**, *50*, 605.
(38) Margoninski, Y.; Kirby, R. E. *J. Phys. C* **1975**, *8*, 1516.
(39) Göpel, W.; Neuenfeldt, G. *Surf. Sci.* **1976**, *55*, 362.
(40) Lubinsky, A. R.; Duke, C. B.; Chang, S. C.; Lee, B. W.; Mark, P. *J. Vac. Sci. Technol.* **1976**, *13*, 189.
(41) Duke, C. B.; Lubinsky, A. R.; Lee, B. W.; Mark, P. *J. Vac. Sci. Technol.* **1976**, *13*, 761.
(42) Duke, C. B.; Lubinsky, A. R.; Chang, S. C.; Lee, B. W.; Mark, P. *Phys. Rev. B: Condensed Matter* **1977**, *15*, 4865.
(43) Duke, C. B.; Meyer, R. J.; Paton, A.; Mark, P. *Phys. Rev. B: Condensed Matter* **1978**, *18*, 4225.
(44) Henrich, V. E.; Zeiger, H. J.; Solomon, E. I.; Gay, R. R. *Surf. Sci.* **1978**, *74*, 682.
(45) Henzler, M. *Surf. Sci.* **1970**, *22*, 12.
(46) Henzler, M. *Surf. Sci.* **1973**, *36*, 109.
(47) Kohl, D.; Henzler, M.; Heiland, G. *Surf. Sci.* **1974**, *41*, 403.
(48) Heiland, G. In "Electrophotographic, International Conference 2nd, 1973"; White, D. R.; Ed.; Society of Photographic Science and Engineering: Washington, DC, 1974; p 117.
(49) Henzler, M. *Appl. Phys.* **1976**, *9*, 11.

mirror electron energy analyzer (CMA) with an integral electron gun for Auger measurements. This system contains an argon sputter gun, LEED optics, a differentially pumped He dc discharge lamp, an X-ray source, and a residual gas analyzer (RGA). The CMA, when run in the retarding mode for UPS, has a constant energy resolution of about 0.2 eV. The dc discharge lamp, which was run at 0.5 torr of He and 0.6 amp, had a ratio of about 400:10:1 for the intensities of the resonance lines at 21.2, 40.8, and 48.4 eV, respectively. The intensity of the UPS signal (about $5 \times 10^3$ counts/s at the maximum of the Zn 3d band) necessitated the use of a signal averager. Single scans of the spectrum took 30 s, and typical spectra were composed of 16 scans. The scanning electron microscope (SEM) used to look at the surface topography was an AMR Model 1400 SEM.

All gases used were research purity with the exception of $NH_3$, which was anhydrous (99.99%). The residual gases observed after bakeout were $H_2$, He, $CH_4$, $N_2$, CO, and Ar.

ZnO crystals were obtained from several sources and varied in bulk conductivities from $10^{-3}$ to 5 $(\Omega\ cm)^{-1}$. The conductivity (bulk plus surface) was found to be adequate to limit charging even at 90 K (the maximum observed shift upon cooling was 0.3 eV for the $(000\bar{1})$ face). The crystals were oriented by X-ray diffraction and then cut into wafers with dimensions of about 6 mm × 6 mm × 1 mm. The (0001) face was distinguished from the $(000\bar{1})$ face by dipping the wafer in HCl; the (0001) face was unaffected while the $(000\bar{1})$ face was rapidly etched by the acid.[50,51] The wafers were polished with 2 μm $Al_2O_3$ grit on a glass plate, followed by further polishing on cloth with 1 μm $Al_2O_3$. After this they were polished with HCl. The concentration (by weight) of the HCl used in this etch was 0.1% for the $(000\bar{1})$ surface and about 10% for the (0001), $(10\bar{1}0)$, and $(11\bar{2}0)$ surfaces. Crystals thus prepared were highly reflecting, with no visible scratches or pits.

These crystals were mounted on a sample holder which could be cooled to 90 K or heated to 1050 K, as measured by a copper–constantan thermocouple. After the samples had been put into the UHV system, they were argon-ion sputtered at 700 K, first for 30 min at 500 V and then for 15 min at 260 V (ion flux density of about 5 $\mu A/cm^2$). This temperature is hot enough for annealing but is below the temperature at which the significant formation of oxygen vacancies is reported to take place.[52] After being sputtered, the surfaces were checked for cleanliness by Auger, then cooled to 90 K and exposed to a $10^{-6}$ torr ambient of CO. The UPS spectra of the CO-covered ZnO surfaces were taken and the amount of adsorbed CO was determined from the area of the CO $4\sigma$ peak. The CO was subsequently pumped out and the samples were reheated to 700 K. At this point the crystal surfaces were again checked for cleanliness, cooled back down to 90 K, and reexposed to CO, and the amount of adsorbed CO was remeasured. This thermal cycling was repeated until the amount of adsorbed CO no longer increased (usually 3 or 4 annealing cycles). If impurities appeared during the annealing, the crystal was sputtered and the thermal cycling repeated. This preparation reproducibly gave surfaces that were atomically cleaned by Auger and exhibited sharp LEED patterns.

LEED measurements were made on all four surfaces at 90 K. For each surface, only integral-order spots were observed, consistent with the literature reports.[28-44] On the polar faces, however, streaks and actual spot-splitting were observed. The splitting of the spots on the (0001) face was sharper than that for the $(000\bar{1})$ face, suggesting[49] that the terrace widths are more regular on the zinc face than on the oxygen face.

In order to obtain the same UPS spectrum of the same face reproducibly, it was necessary to orient the crystal in front of the CMA in exactly the same manner each time. This sensitivity arises from the strong angular anisotropy in the angular distribution of the emitted photoelectrons,[53] coupled with the acceptance geometry of the CMA. The CMA accepts electrons in a cone with a half angle of 42.3 ± 3° for a full 360° about the CMA axis (with the exception of supports used to separate the inner and outer cylinders, which block four evenly spaced segments of approximately 8° each). The incident photon beam is fixed with respect to the CMA, is unpolarized, and is at an angle of 75° from the CMA axis. The crystals were mounted on the sample holder in an orientation which reproduced the azimuthal direction about the surface normal with respect to the photon direction with an angle of 5° between the surface normal of the crystal and the CMA axis, with the surface normal tilted toward the photon source.

For the limited angle-resolved measurements which utilized this UPS system, the acceptance cone of the CMA was masked with a stainless-steel plate with a hole in it. The plate could be positioned in front of the CMA from outside the UHV system, with the hole either in the direction toward the photon source or 180° away from it. The dimensions of the hole were such that the detector would accept a 6° circular solid angle.

Scanning electron microscope (SEM) photographs were taken of the $(10\bar{1}0)$ and (0001) faces after surface preparation and subsequent removal from the vacuum system. The SEM photographs of both surfaces showed scratches in low magnifications, but there was no observable surface roughness up to a magnification of 23 000.

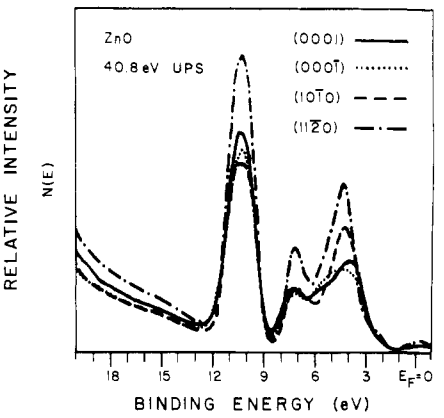


**Figure 2.** 40.8-eV UPS spectra of the four low-index surfaces of ZnO. Fermi level ($E_F$) obtained from gold is defined as zero. Relative intensities have been determined from measurements of physisorbed $NH_3$.

## Results and Discussion

**A. He II UPS Spectra of the $(10\bar{1}0)$, $(11\bar{2}0)$, (0001), and $(000\bar{1})$ Clean Surfaces of ZnO.** After a surface had been prepared and characterized by Auger and LEED, the He II UPS spectrum was taken of the clean surface at 90 K. The spectra of the four ZnO surfaces are shown in Figure 2. The Fermi level was determined from UPS spectra of a piece of gold foil on the sample holder; it is used as a reference level for all the spectra presented here. Three dominant features are observed in the UPS spectrum of ZnO. The first peak in the spectrum from 3 to 6 eV is due to O 2p nonbonding electrons; the peak from 6 to 8.5 eV is due to the bonding combination of Zn 4s and 4p with O 2p electrons; and the intense peak from 8.5 to 12 eV is due to the Zn 3d band.[54-56] The position of the low binding energy edge of the valence band below the Fermi level is dependent upon the band gap, as well as any surface charging or any band bending (due to chemisorbed or ionosorbed surface species). The spectra in Figure 2 have been aligned to compensate for variations in these effects between surfaces. Finally, the weak shoulder on the low binding energy side of the valence band is due to the line at 48.4 eV, which has about 10% of the intensity of the line at 40.8 eV.

Due to the strong polarization-dependent anisotropy in the distribution of photoelectrons (vide infra), the relative intensity measured for each peak is dependent upon the detection geometry and photon polarization. In order to compare the relative intensities of the clean spectra of the four surfaces, we needed some means of scaling the data. This was achieved by exposing the surfaces at 90 K to 1000 L (1 L = 1 langmuir = $10^{-6}$ torr s) of $NH_3$, which resulted in many layers of physisorbed $NH_3$. The physisorbed $NH_3$ spectrum was the same on all four surfaces, indicating that the $NH_3$ photoemission was essentially isotropic and that no ZnO photoelectrons were being detected. The measured $NH_3$ spectra could then be scaled to each other, resulting in a calibration factor for the clean ZnO spectra. The UPS spectra in Figure 2 have been scaled by this factor.

Finally, the UPS spectra of the four clean surfaces were measured as a function of temperature and found to be invariant. This justifies the use of a clean spectrum measured at 90 K as a background for subtraction from the spectra obtained after

(50) Klein, A. *Z. Phys.* **1965**, *188*, 352.
(51) Heiland, G.; Kunstmann, P. *Surf. Sci.* **1969**, *13*, 72.
(52) Göpel, W. *J. Vac. Sci. Technol.* **1978**, *15*, 1298.
(53) Orchard, A. F. In "Electronic States of Inorganic Compounds: New Experimental Techniques"; Day, P., Ed.; D. Reidel Publishing Co.: Boston, 1975; p 267.
(54) Tossell, J. A. *Chem. Phys.* **1976**, *15*, 303.
(55) Tossell, J. A. *Inorg. Chem.* **1977**, *16*, 2944.
(56) Kowalski, J. M. Masters Thesis, Department of Material Science and Engineering, MIT, Cambridge, MA, 1978.

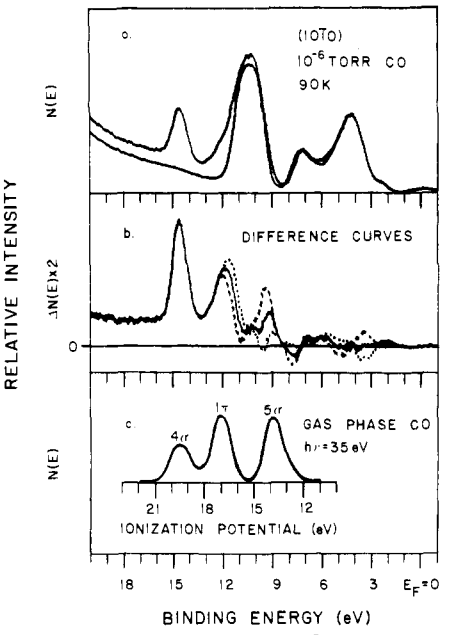


**Figure 3.** (a) 40.8-eV UPS spectrum of the (10$\bar{1}$0) surface at 90 K before and after exposure to a $10^{-6}$ torr ambient of CO (the clean spectrum has been attenuated and shifted to maximize overlap in the oxygen valence region). (b) Difference curve between exposed and clean spectrum in a (—) showing the effect of a +100-meV (···) and −100-meV (- - -) shift of the clean spectrum. (c) 35-eV UPS spectrum[27,57] of gas-phase CO.

exposure to a gas for a range of temperatures. The effects of an exposure to CO at various temperatures and pressures will now be considered.

**B. The He II UPS Spectrum of the CO/ZnO (10$\bar{1}$0) Surface Complex.** The UPS spectrum obtained from the (10$\bar{1}$0) surface in $10^{-6}$ torr ambient of CO at 90 K is presented in Figure 3a (a clean surface spectrum has been included for comparison). It was found that the spectrum of the CO-exposed surface was dependent upon the ambient CO pressure and *not* upon the extent of the exposure; further, it had a very marked dependence upon the sample temperature. That the measured spectrum was characteristic of a truly reversible equilibrium between the amount of adsorbed CO and the gas-phase concentration was determined by approaching the equilibrium from the lower coverage and higher coverage directions and obtaining the same spectrum. Thus, a clean surface exposed to a $10^{-6}$ torr ambient of CO gave the same UPS spectrum as was obtained in the same ambient pressure after having increased the ambient pressure to $10^{-5}$ torr and having observed an increase in the CO $4\sigma$ intensity.

In Figure 3a, the clean ZnO UPS spectrum has been attenuated and shifted to maximize the overlap in the oxygen valence band region. The attenuation is required since the layer of adsorbed CO decreases the photoelectron intensity coming from the ZnO. A shift of the spectrum can come from a change in the amount of charging or the amount of band bending after adsorption. Further, maximal overlap of the valence band region is used rather than alignment of the low binding energy edge of the valence band since it is possible that adsorption could effectively shift this edge by depleting surface states. If the clean surface spectrum is then subtracted from the spectrum of CO on ZnO, the difference curve in Figure 3b is obtained. Since there is no unambiguous way of aligning the raw data before taking the difference, the effect of a ±100 meV shift of the background is also shown. These shifts cause large changes in both the shapes and apparent positions of the $1\pi$ and $5\sigma$ peaks. However, the shape and position of the $4\sigma$ peak remain invariant with these shifts. In Figure 3c the 35-eV gas-phase UPS spectrum of CO[27,57] has been shifted to align the $4\sigma$ peak with the difference peak at 14.6 eV.[58] From this alignment, the other two peaks in the difference curves, at about 12 and 9.5 eV, may be assigned to the $1\pi$ and $5\sigma$ orbitals of CO, respectively. While the position of the $5\sigma$ orbital is difficult to determine accurately, a decrease in the energy of the $4\sigma$–$5\sigma$ splitting of at least 0.5 eV relative to the free CO molecule is seen in the difference curves of Figure 3b. Further, as the intensity of the CO $4\sigma$ peak is not influenced by the manner in which the difference curve is taken, it can be used as a direct probe of the amount of CO adsorbed on the surface.

**C. Evidence for Undissociative CO Chemisorption to Clean Terrace Sites on the (10$\bar{1}$0) Surface.** It should first be noted that while the 42 photoelectron only probes the undissociated CO molecule, the possibility of a measurable amount of dissociated CO on the surface can be excluded. Warming the CO-exposed (10$\bar{1}$0) surface to ~200 K produces a ZnO valence band spectrum identical with the original 90 K clean surface spectrum. Since UPS is sensitive to effects having $\theta \geq 0.05$, it can be concluded that any dissociative effects have $\theta < 10^{-2}$, in agreement with the findings of other researchers.[59,60]

Several types of evidence indicate that this CO is adsorbing to reasonably well-defined (10$\bar{1}$0) terraces rather than steps, imperfections, or vacancy surface sites. First, measurements of the intensity of the CO $4\sigma$ peak were used to study the effects of various surface preparations upon the amount of CO which would adsorb. The argon-ion sputtering (260 V for 30 min) of a previously prepared surface caused the LEED patterns to become more diffuse and reduced the amount of CO that the surface would adsorb to about half of its previous level. This decrease implies that the highest adsorption is a property of a well-structured surface and is not only due to adsorption at defects. Also, it is possible to prepare a surface with a significant content (4% of sites) of oxygen vacancies by heating in vacuo at 1050 K for 180 s.[60] This preparation produced no measurable change in the $4\sigma$ intensity when subsequently cooled and exposed to CO. Further, by comparing the integrated area under the CO $4\sigma$ peak with that of the Zn 3d band, it is possible to estimate[61] the coverage as being close to a monolayer at 90 K and $10^{-6}$ torr ambient of CO. Finally, the continuous decrease of the heat of adsorption on coverage and the marked dependence of the $4\sigma$ intensity on angle, with a sharp peak at 30° off the surface normal (vide infra) strongly support well-formed terrace surface sites for CO adsorption on (10$\bar{1}$0).

Previous reports have indicated that the adsorption of CO on ZnO is sensitive to preexposure of the surface to $H_2$ or $O_2$,[62] and UPS measurements on ZnO (10$\bar{1}$0) surfaces have indicated that CO would adsorb only in the presence of $H_2$.[27] However, we could observe no changes in the amount of CO which would adsorb to any of the four surfaces due to the presence of $H_2$, whether the surfaces were exposed to $H_2$ previous to or concurrently with the CO exposure. Similarly, there was no effect upon the spectra when the surfaces were preexposed to $O_2$ or when $O_2$ was mixed with the CO ambient.

**D. He II UPS Studies of $NH_3$ Competition with CO for ZnO Surface Sites.** In contrast to $H_2$ and $O_2$, which neither adsorbed to any large extent on the clean ZnO surfaces (i.e., did not alter the 40.8-eV UPS spectra of the clean ZnO) nor affected the CO/ZnO spectra, $NH_3$ did both. $NH_3$ was found to chemisorb on all four clean surfaces, and at low temperatures (below 120 K) it physisorbed (condensed), completely eliminating any features due to the ZnO. The chemisorbed form remained on the surface up to about 450 K. The temperature of desorption indicates a heat of adsorption substantially higher than that of CO.

If a prepared (10$\bar{1}$0) surface was in equilibrium with a $10^{-6}$ torr ambient of CO, and a trace amount ($10^{-9}$ torr) of $NH_3$ was let into the system (monitored on a precalibrated RGA), this $NH_3$

(57) Lüth, H.; Rubloff, G. W.; Grobman, W. D.; International Business Machines Corporation, Thomas J. Watson Research Center, personal communication, 1978.

(58) This alignment of the CO corresponds to an extramolecular relaxation/polarization shift of about 0.7 V.

(59) Hotan, W.; Göpel, W.; Haul, R. *Surf. Sci.* **1979**, *83*, 162.

(60) Göpel, W.; Bauer, R. S.; Hansson, G. *Surf. Sci.*, in press.

(61) Estimation based on formulas presented in: Henrich, V. E.; Dresselhaus, G.; Zeiger, H. J. *Phys. Rev. B: Condensed Matter* **1978**, *17*, 4908.

(62) Hayward, D. O.; Trapnell, B. M. W. "Chemisorption", 2nd ed.; Butterworth & Co.: Washington, DC, 1964.

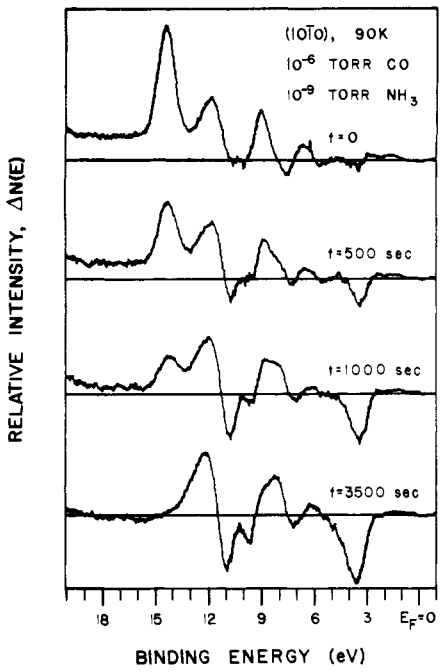


**Figure 4.** Difference curves showing the competition on the (10$\bar{1}$0) surface between $10^{-6}$ torr of CO and $10^{-9}$ torr of $NH_3$. The length of time of exposure to the $NH_3$ is indicated on each curve.

displaced the adsorbed CO, as may be seen in Figure 4. The features in the difference curve for $t$ = 3500 s are due to chemisorbed $NH_3$. The figure is for the (10$\bar{1}$0) face, but qualitatively the same effect was observed on all four surfaces.

$NH_3$, a Lewis base, should interact strongly with the acidic Zn(II) sites.[63] The displacement of the adsorbed CO by $NH_3$ demonstrates the strong involvement of zinc ions in the CO binding. Further, both $NH_3$ and CO can be seen to sharpen the Zn 3d band upon exposure, although to a greater degree in the case of $NH_3$. This may be interpreted in terms of variation in a Zn 3d surface state and will be treated in more detail elsewhere,[64] but the similarity is consistent with the negative end of the adsorbed CO molecule bonding to a zinc surface ion.

**E. He II UPS Studies of the CO Equilibrium on the (10$\bar{1}$0), (11$\bar{2}$0), (0001), and (000$\bar{1}$) Surfaces of ZnO.** In order to probe the specific surface geometric requirements for chemisorption further, we measured the CO/ZnO equilibrium coverage as a function of temperature and pressure on each of the four low-index surfaces by using the He II 4$\sigma$-electron intensity, and an appropriate isobar was fit to the observed equilibrium values to obtain the heat of adsorption on each surface. The pressures used were $10^{-6}$ and $10^{-8}$ torr, and the temperature was varied. Both the original spectra and the difference curves for the $10^{-6}$ torr ambients are shown in Figure 5 for the two polar surfaces and in Figure 6 for the two nonpolar surfaces. By measuring the area of the 4$\sigma$ peak as a function of temperature and pressure, the isosteric heat of adsorption ($\Delta H_{ads}$) can be determined from the Clausius–Clapeyron equation (2). Such a determination of the heat

$$\left(\frac{\partial \ln P}{\partial(1/T)}\right)_\theta = -\frac{\Delta H_{ads}}{R} \quad (2)$$

of adsorption for any of the four faces indicates that $\Delta H_{ads}$ decreases with increasing coverage. This indicates either that the surface adsorption sites are heterogeneous (which was argued against earlier) or that there is a repulsive adsorbate–adsorbate interaction. For a repulsive adsorbate–adsorbate interaction, the $\Delta H_{ads}$ should be a continuous function of surface coverage, $\theta$,[65] and in particular a linear decrease can derive from dipole–dipole repulsions.[66] In Figure 7 the area of the 4$\sigma$ peak has been plotted for the two pressures as a function of temperature. These points were then fit with a Temkin isobar, which is a Langmuir isotherm plotted as an isobar with a linear dependence of $\Delta H_{ads}$ upon coverage:[62]

$$\Delta H_{ads}(\theta) = \Delta H_0(1 - \alpha\theta) \quad (3)$$

where $\Delta H_0$ = the heat of adsorption at zero coverage. Thus

$$\frac{\theta}{1-\theta} = kP \exp[\Delta H_0(1 - \alpha\theta)/RT] \quad (4)$$

where $k$ is a proportionality constant determined by estimating values for $\theta$, determining $\Delta H_{ads}(\theta)$ from the Clausius–Clapeyron equation, and solving for $k$, giving a value of about $4.0 \times 10^{-9}$. Equation 4 can then be solved iteratively to determine relative values of $\theta$ as a function of $T$ at constant $P$. The fit to the data based on continuous variation in the heat of adsorption is quite good but does not preclude the possibility of surface heterogeneity. In either case, $\Delta H_0$ is found to be 12.0 ± 0.4 kcal/mol for all four surfaces, indicating that the adsorption sites are the same or very similar on all four surfaces.

Since the adsorption is never observed to reach saturation, it is not possible to determine $\theta$ accurately; however, it is estimated[61] to be close to a monolayer. With the assumption that the adsorbate–adsorbate interaction, as reflected by $\alpha$, is about the same on all four surfaces, the Temkin isobars that were used to fit the experimental points can be extrapolated to lower temperatures and to saturation coverage. The dotted portions of Figure 7 present this approximation. The values of $\alpha$ would indicate that the heat of adsorption drops from 12.0 kcal/mol at zero coverage to 6 kcal/mol at 90 K and extrapolates to about 5 kcal/mol at unity coverage.

The data points shown in Figure 7 were scaled so that the intensities from the four faces could be compared directly. This was accomplished by first scaling the data to the relative intensities of the four clean spectra shown in Figure 2, followed by further scaling of the data to the area of a surface unit cell (since the detector measures a constant area, more signal would be observed from a surface with a smaller surface unit cell) and then scaling to 1000 for the (10$\bar{1}$0) surface. The observed intensities for the two nonpolar faces are significantly larger than those for the two polar faces. The relative intensities, extrapolated to unity coverage, are 1700 (11$\bar{2}$0):1000 (10$\bar{1}$0):390 (0001):230 (000$\bar{1}$).

Two important observations may be derived from the data presented in Figure 7. The first is that CO has about the same $\Delta H_0$ on all four surfaces. This requires that the CO-surface bonding interaction be quite similar on all four. The second is that the relative intensities of the 4$\sigma$ peaks on the nonpolar surfaces are larger than on the polar surfaces with the (0001) zinc face having significantly higher 4$\sigma$ intensity than the (000$\bar{1}$) oxide surface. Since the CO-surface bond is quite similar for the four surfaces, these differences in the 4$\sigma$ intensity must be explained in terms of variation both in the number of similar sites and in the orientation of the CO molecule bound to these sites with respect to the electron analyzer. The latter effect arises because the photoelectron intensity distribution from the CO 4$\sigma$ orbital is extremely anisotropic, with the dominant intensity directed axially out of the oxygen end of the molecule, and the CMA detects with only a limited acceptance angle as described in the Experimental Section.

**F. Angle-Resolved He II UPS Studies of CO on ZnO Surfaces.** Although these CO orientation effects complicate a comparison of the integrated 4$\sigma$ intensities on the four surfaces, they do allow a fairly detailed determination of the binding orientation for CO on ZnO when studied directly. Thus, angle-resolved He II UPS measurements have been employed in determining this orientation on the (10$\bar{1}$0) and (0001) surfaces.

Initially, limited angle-resolved measurements were performed on the (10$\bar{1}$0) surface as described in the Experimental Section.

(63) Morrison, S. R. *Surf. Sci.* **1975**, *50*, 329.
(64) Gay, R. R.; Solomon, E. I.; Henrich, V. E.; Zeiger, H. J., to be submitted for publication.
(65) Aristov, B. G.; Bezus, A. G.; Berezin, G. I.; Sinitsyn, V. A. *Osnovn. Probl. Teor. Fiz. Adsorbtsii, Tr. Vses. Konf. Teor. Voprosam Adsorbtsii 1st* **1970**, 367.
(66) Roberts, J. K. *Trans. Faraday Soc.* **1938**, *34*, 1342.

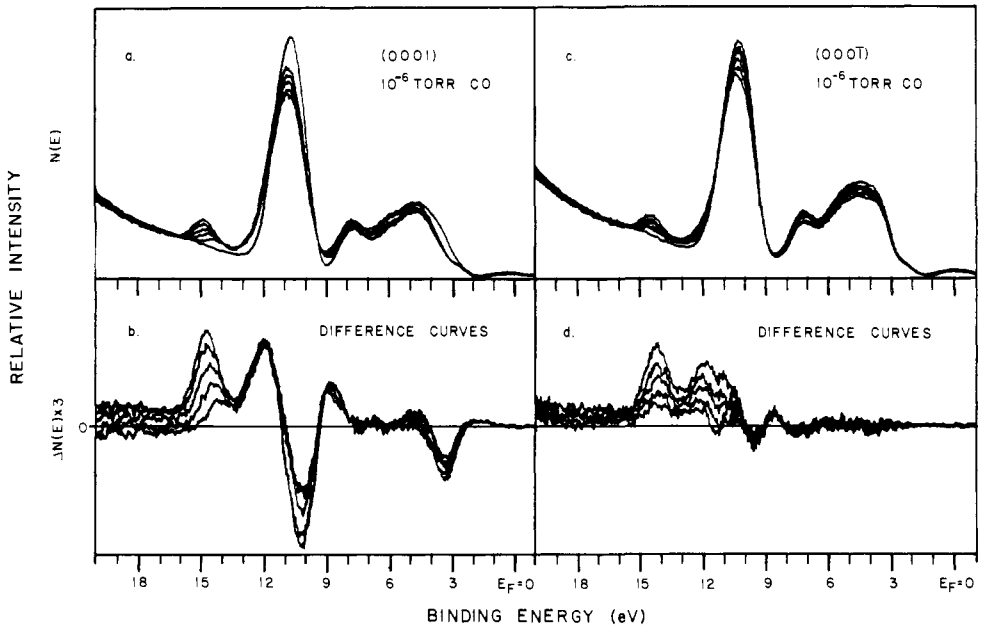


**Figure 5.** He II UPS spectra of the polar surfaces of ZnO in a $10^{-6}$ torr ambient of CO as a function of temperature. The clean spectra have been included for comparison: (a) (0001) surface, (b) (0001) difference curves, (c) (000$\bar{1}$) surface, (d) (000$\bar{1}$) difference curves. The difference curves have been obtained by aligning the clean spectra to maximize overlap in oxygen valence band.

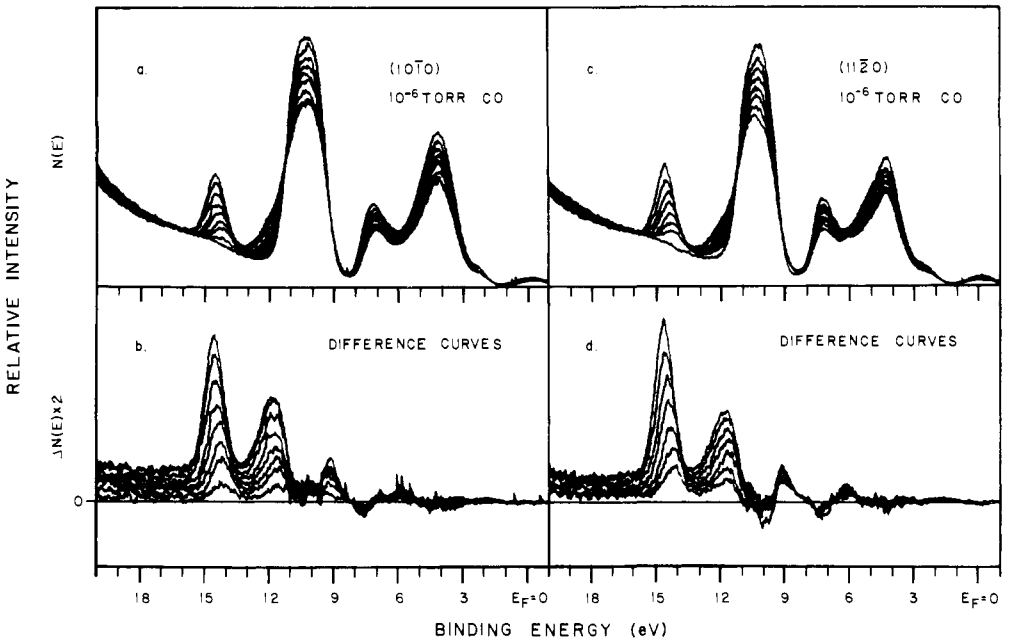


**Figure 6.** He II UPS spectra of the nonpolar surfaces of ZnO in a $10^{-6}$ torr ambient of CO as a function of temperature. The clean spectra have been included for comparison: (a) (10$\bar{1}$0) surface, (b) (10$\bar{1}$0) difference curves, (c) (11$\bar{2}$0) surface, (d) (11$\bar{2}$0) difference curves. The difference curves have been obtained by aligning the clean spectra to maximize overlap in the oxygen valence band.

The direction of a vector in the coordinate system used here is given by the polar angle, $\theta$, which it makes with respect to the CMA axis, and the azimuthal angle, $\phi$, which is referenced to the direction of the photon source. The UPS spectra for two angular directions were measured for each crystal alignment. The orientation of the CMA axis, photon source, and measured directions are shown in Figure 8. The alignment of the crystal is given by the direction of the surface normal and an orientation of the crystal about the surface normal, specifying the direction of the $c$ axis. Three angle-resolved measurements were made on the (10$\bar{1}$0) surface. The orientations of the crystals and the ratio of the intensity measured at $\phi = 0$ to that at $\phi = 180$ are listed in Table I. The crystal orientation for experiment no. 1 is indicated in Figure 8, and the angle-resolved photoelectron data are presented in Figure 9. These limited angle-resolved data on the (10$\bar{1}$0) surface clearly show a large $4\sigma$ intensity when the detector is oriented along the coordinatively unsaturated direction

Table I. Crystal Orientations and Measured CO $4\sigma$ Intensity Ratios

| expt no | cryst face | directn of surface normal $\theta, \phi$ (degs) | orientatn about surface normal $\theta, \phi$ (deg) | measd $I(\phi = 0):I(\phi = 180)$ |
|---|---|---|---|---|
| 1 | 10$\bar{1}$0 | 5, 0 | 95, 0 | 1:>10 |
| 2 | 10$\bar{1}$0 | 5, 0 | 85, 180 | 2.5:1 |
| 3 | 10$\bar{1}$0 | 5, 180 | 95, 180 | 1.4:1 |

of the zinc ion but only a very low $4\sigma$ intensity of electrons emitted along the coordinatively unsaturated direction of the oxide ion. Since this anisotropy directly relates to the CO molecular axis, this defines the CO to be bonding to the (10$\bar{1}$0) surface with one of the two geometries indicated at the top of Figure 10. In order to differentiate between these two models, one may use the observed decrease in the splitting of the energies of the $4\sigma$ and $5\sigma$

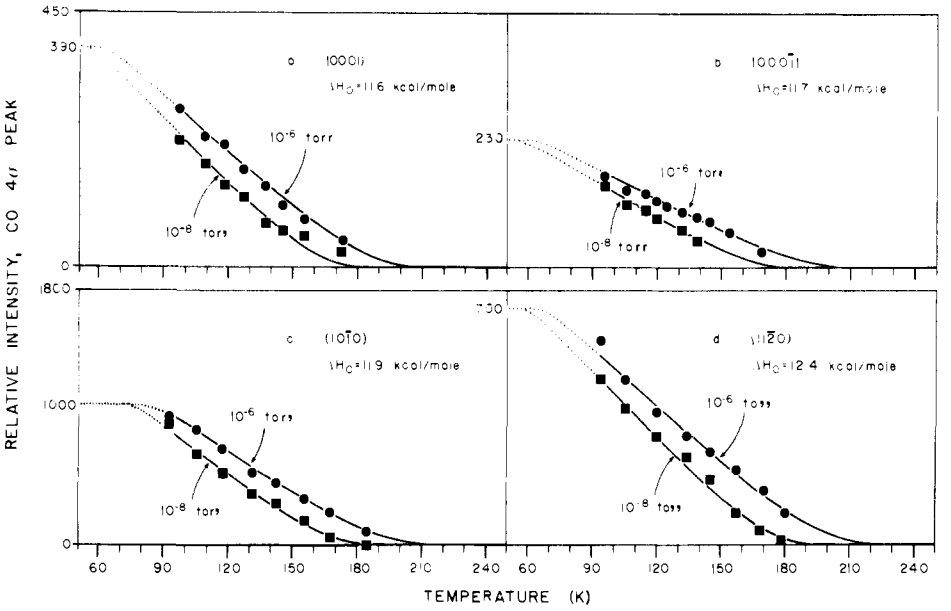


**Figure 7.** Variation in the equilibrium coverage of CO on the four ZnO surfaces as a function of temperature and pressure as measured by the $4\sigma$ intensity. Data have been fit to a Temkin isobar; extrapolated values are indicated with a dotted line. Data have been scaled to the relative intensities of the clean spectra and the size of a surface unit cell. Note the different scale for a and b from that for c and d.

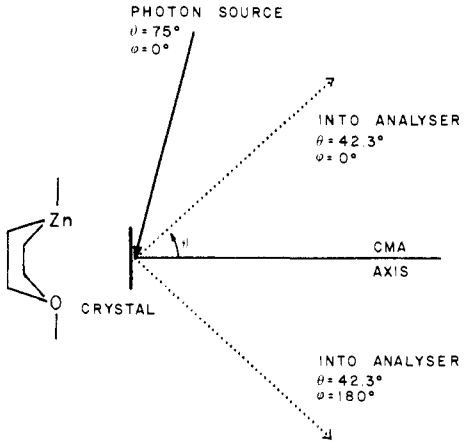


**Figure 8.** Geometry used for the angle-resolved measurements, showing the two detection directions measured.

molecular orbitals. Bonding interactions between the $Zn^{2+}$ ion and the electrons closest to this ion should stabilize these electrons relative to the rest of the molecule. However, interactions with the $O^{2-}$ ion should have a destabilizing influence. The relative molecular orbital energies to be expected for the two possible CO binding models are shown at the bottom of Figure 10. For the O-bound geometry, the splitting between the $4\sigma$ and $5\sigma$ orbitals should *increase* while for the C-bound geometry it should *decrease*, which is what is observed. This then implies the C-bound geometry of Figure 10a.

Recently, we have completed detailed angle-resolved studies on the (10$\bar{1}$0) and (0001) surfaces in collaboration with McFeely et al.[67,68] These studies employed S- and P-polarized He II photons and CO $4\sigma$ photoemission detection at every 10° both in and out of the incident plane. For the (10$\bar{1}$0) surface, these studies have allowed a reasonably accurate determination of the angle $\alpha$ in Figure 10a as approximately 30°. Further, for the (0001) surface, these studies have indicated that the CO molecules are oriented normal to the surface with a $4\sigma$ angle-resolved intensity of ~70% that of the angle-resolved $4\sigma$ intensity on the (10$\bar{1}$0) surface. Thus, the apparent decrease in $I_{4\sigma}$ of the CO

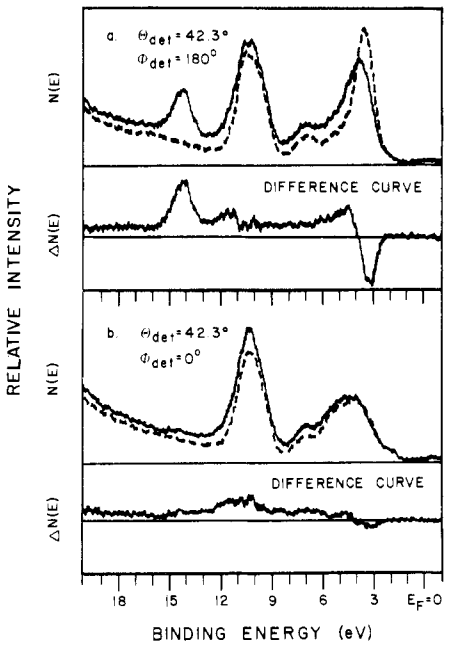


**Figure 9.** Angle-resolved spectra and difference curves for the (10$\bar{1}$0) surface. Crystal surface normal at $\theta = 5°$, $\phi = 0°$, and $c$ at $\theta = 95°$, $\phi = 0°$. Clean (---) and CO covered (—) spectra are shown for the detector at (a) $\theta = 42.3°$, $\phi = 180°$ and (b) $\theta = 42.3°$, $\phi = 0°$. The spectra were taken at 90 K, for a $10^{-6}$ torr ambient of CO.

molecule on the (0001) as compared to the (10$\bar{1}$0) surface in Figure 7 simply reflects a relatively poor orientation of the CO molecule on the coordinatively unsaturated zinc terrace sites with respect to the fixed CMA electron detection angle.

An analogous CO orientation effect would readily account for the increased $4\sigma$ intensity on the (11$\bar{2}$0) surface (Figure 7). For this surface, CO molecules oriented on sites analogous to those on the (10$\bar{1}$0) face would make an angle $\alpha$ of 41.4° with respect to the surface normal, and further form two surface domains. Alternatively, the low but nonzero $4\sigma$ intensity on the (000$\bar{1}$) surface cannot be explained by orientation effects on nondefect terrace sites. Only coordinatively unsaturated oxide ions are accessible yet all the previous experiments demonstrate CO binding carbon end to coordinatively unsaturated zinc ions. At this point, the most reasonable explanation for the (000$\bar{1}$) $I_{4\sigma}$ results requires adsorption to zinc ions on the (10$\bar{1}$0) surfaces exposed on the steps,

(67) Sayers, M. J.; McClellan, M. R.; Gay, R. R.; Solomon, E. I.; McFeely, F. R. *Chem. Phys. Lett.*, in press.
(68) McClellan, M. R.; Trenary, M. W.; Shinn, N. D.; D'Amico, K. L.; Sayers, M. J.; Solomon, E. I.; McFeely, F. R., to be submitted for publication.

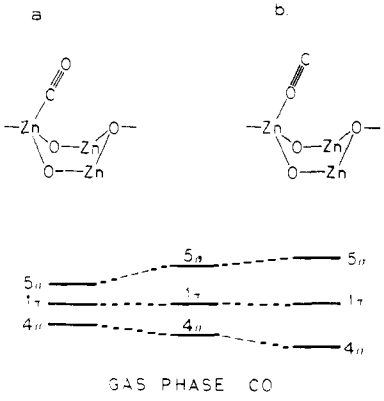


**Figure 10.** Possible CO binding geometries consistent with the limited angle-resolved measurements. A schematic representation of the expected molecular orbital splitting patterns is shown for each geometry.

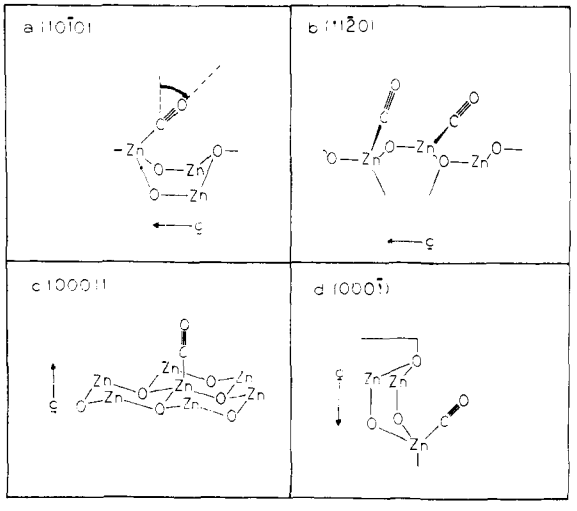

**Figure 11.** Approximate model of the active site for chemisorption of CO on the four ZnO surfaces.

which are known to be present from the LEED measurements on these surfaces, although detailed angle-resolved UPS measurements are necessary to confirm this. Thus, the active sites for CO chemisorption on the two nonpolar and two polar surfaces of ZnO are shown in Figure 11.

**G. He I UPS Studies of CO on the (10$\bar{1}$0), (11$\bar{2}$0), (0001), and (000$\bar{1}$) Surfaces of ZnO.** The CO/ZnO system was also studied by using the He I emission line (21.2 eV) as the exciting source. Figure 12 shows the He I spectra corresponding to the He II spectra shown in Figure 3. Due to both the large inelastically scattered tail and the low cross section of the CO 4$\sigma$ orbital to photoionization at these energies, the technique of looking at difference spectra proved to be unfruitful. However, by biasing the sample relative to the detector, it was possible to measure both the onset of the inelastic electron tail which contains information about the photoemissive work function and the position of the edge of the valence band, which gives an indication of the amount of band bending present. While the absolute value of either function is difficult to determine accurately (±0.1 eV), the changes in the values can be readily determined, provided the shape of the UPS spectrum has not significantly changed. These differences were measured by scaling the spectra to a common maximum intensity and averaging together the differences in energy at different heights on the curve. For a semiconductor surface, the total change in the work function arises from two contributions, one due to the presence of an adsorbed dipolar layer and the other due to a change in the band bending. Thus

$$\Delta\phi_{total} = \Delta\phi_{dipole} + \Delta\phi_{bb} \quad (5)$$

Since the He I spectrum allows the direct measurement of $\Delta\phi_{total}$ and $\Delta\phi_{bb}$, the dipole moment contribution can be determined by

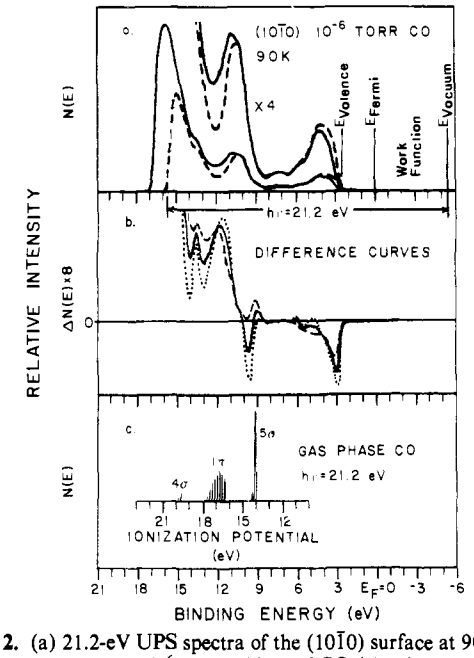


**Figure 12.** (a) 21.2-eV UPS spectra of the (10$\bar{1}$0) surface at 90 K before and after exposure to a $10^{-6}$ torr ambient of CO (the clean spectrum has been attenuated and shifted to maximize overlap in the oxygen valence band region). (b) Difference curve between exposed and clean spectra in a (—), showing the effect of a +100-meV (···) and -100-meV (- - -) shift of the clean spectrum. (c) 21.2-eV UPS spectrum[71] of gas-phase CO, aligned as in Figure 3.

difference. A negative value of $\Delta\phi_{dipole}$ is found for all four faces, which corresponds to an orientation in which the dipole $E$ vector is pointed toward the surface, i.e., with the negative side of the dipole down, implying some charge transfer to the surface.

As long as no adsorption-induced surface reconstruction occurs (vide infra) the value of $\Delta\phi_{dipole}$ should directly reflect the amount of CO on the surface. Since the intensity of the 4$\sigma$ orbital also reflects this amount, it should be possible to fit the temperature and pressure dependence of the $\Delta\phi_{dipole}$ to a Temkin isobar with the same thermodynamic parameters as for the 4$\sigma$ intensity, allowing only for a change in the scale factor. Figure 13 shows that this is indeed the case. As before, the change is significantly smaller on the (000$\bar{1}$) face. Knowing the coordination geometry of the CO at the (10$\bar{1}$0) surface active site, it is possible to estimate a value for the dipole moment of the adsorbed CO complex by using the Helmholtz equation[62,69]

$$\mu = \Delta\phi_{dipole}/4\pi n_s\theta \cos\beta \quad (6)$$

where $\mu$ = dipole moment of the CO molecule, $n_s$ = number of molecules adsorbed/cm$^2$ of surface and $\beta$ is the angle the CO makes relative to the surface normal. When this calculation is performed for the (10$\bar{1}$0) face, it yields a value $\mu = 0.61 \pm 0.11$ D. This is significantly higher than the gas-phase value of 0.112 D.[70]

The calculation can also be performed for the other faces. The (11$\bar{2}$0) face also yields a value of 0.59 ± 0.12 D. Since the (11$\bar{2}$0) surface is known not to reconstruct, the fact that the dipole moment is the same is a good argument that there is no change in the relaxation on the (10$\bar{1}$0) face upon chemisorption. However, the (0001) face results in a dipole moment of 0.19 ± 0.05 D. This anomalously small figure can be explained by assuming either that only about one-third of the sites on the zinc face are occupied at the point where the isobar levels off or that some kind of interfering process is taking place which is creating a spurious dipole moment. The former possibility seems to be ruled out since the angle-resolved 4$\sigma$ intensity indicates that the (0001) face has at least 70% of the amount adsorbed on the (10$\bar{1}$0) face. Moreover, there is additional evidence to argue for some competing factor. In

(69) Stern, O. *Z. Elektrochem.* **1924**, *30*, 508.
(70) U. S. National Bureau of Standards, Report NSRDS-NBS 10.
(71) Turner, D. W.; Baker, C.; Baker, A. D.; Brundle, C. R. "Molecular Photoelectron Spectroscopy"; Wiley-Interscience: New York, 1970; p 49.

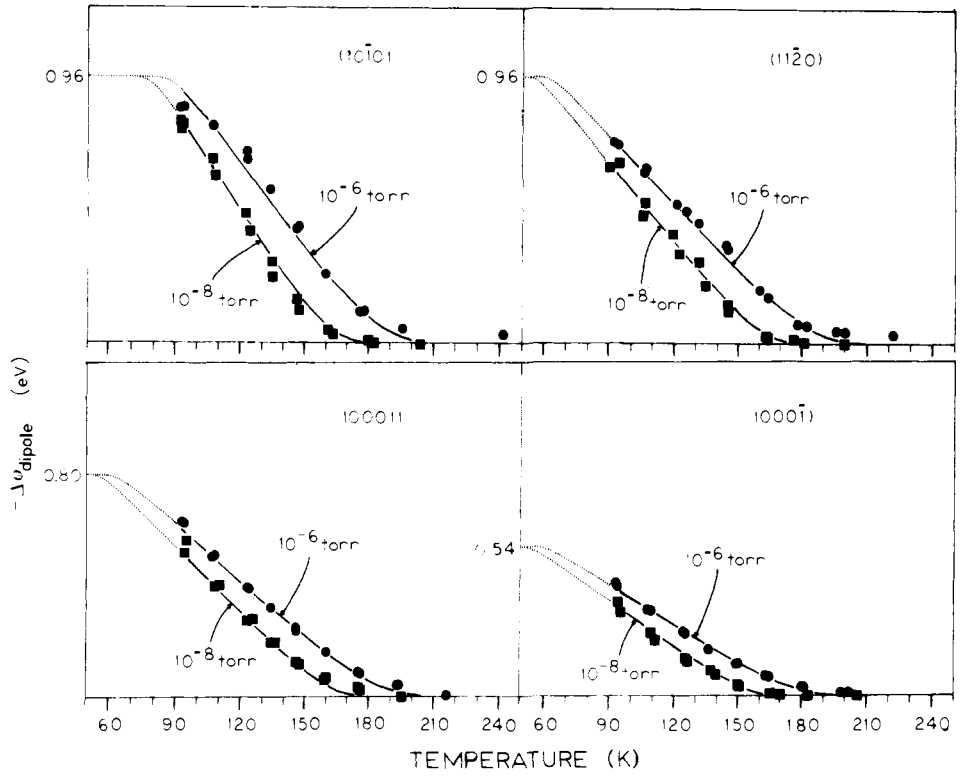


**Figure 13.** Variation in the dipole contribution of the work function on the four ZnO surfaces as a function of temperature and pressure. Data have been fit to a Temkin isobar; extrapolated values are indicated with a dotted line. All data are on the same scale.

contrast to the behavior on the other three faces, when a (0001) face that has been exposed to CO is warmed to ~200 K so that the $4\sigma$ intensity goes to zero, neither the He I nor He II spectra return to the original clean spectra taken before the exposure. One possibility for this difference is that the CO molecules may cause the zinc ions which are relaxed into the threefold sites by 0.3 Å on the clean surface to experience an unrelaxation which may be frozen in at the still low temperatures at which the CO $4\sigma$ intensity disappears. Another possibility is that there is also a dissociated form of CO which adsorbs only on the (0001) zinc face. It is possible to distinguish between these processes by measuring the CO/ZnO spectra at temperatures where only a small amount of CO will adsorb (173 K) by using both a clean surface and one that has been preexposed to CO. When this is done, all the features appearing on the clean spectrum are seen to be proportional to coverage, as opposed to the difference curves shown in Figure 5 for the (0001) face where the only peak proportional to the coverage is the $4\sigma$. This would argue that the change is caused by some effect such as an unrelaxation, which would take place at high coverages, rather than being due to some small amount of dissociated CO on the surface. In any event, heating the crystal to annealing temperatures (700 K) is sufficient to restore the original clean spectrum.

**H. Other Surface Techniques Explored.** Finally, the applicability of a number of other surface sensitive techniques has been explored. X-ray photoelectron spectra of the ZnO valence band region, using 1254 eV photons, exhibited predominantly the Zn 3d band, with only a weak oxygen valence band, both before and during exposure to a $10^{-6}$ torr ambient of CO. This is due to the low cross section for photoionization of delocalized states by high-energy photons.[72] Furthermore, it was not possible to observe the C 1s level after adsorption, either because it falls in the region of the Zn Auger transitions, which obscure it, or because satellite structure causes the band to be too broad to be observed. The LEED patterns were monitored as CO was introduced into the system, and no superstructure was observed. However, the primary spot patterns became diffuse and the contrast between spots and background decreased. Furthermore, if CO was adsorbed on the clean surface, the carbon could not be detected by Auger, due either to local heating of the crystal or to electron-stimulated desorption. Attempts to look at the adsorbed CO by energy-loss spectroscopy led to decomposition of the CO and the deposition of carbon on the surface.

## Summary

The data obtained in this study support the CO/ZnO-idealized active site structures represented in Figure 11 for the four single crystal surfaces. These sites involve a dominant interaction of CO with the coordinatively unsaturated zinc surface ions. This is supported by (1) the fact that $\Delta H_{ads}$ is the same on all four surfaces, (2) the ammonia competition experiments ($NH_3$ displaces CO), (3) the relative He II UPS $4\sigma$ intensities on the four single crystal surfaces (lowest on the (000$\bar{1}$) oxide surface), and (4) the angular dependence of the $4\sigma$ intensity (which shows the CO axis is oriented close to the coordinatively unsaturated direction of the surface zinc ion). Further, CO binding carbon end to the zinc is indicated by the decrease in the $4\sigma$–$5\sigma$ splitting relative to that of the free CO molecule.

The electronic structure of this CO/ZnO active site complex seems to be dominated by weak $\sigma$ donor and little or no $\pi$-acceptor interactions with the zinc ion. This is derived from the ~0.5-eV stabilization of the $5\sigma$ orbital (approximately a lone pair on the carbon) and from the increase in the dipole moment of the CO adsorption complex to ~0.6 D indicative of some net electronic donation from the carbon to the surface, resulting in a positive charge on carbon. This is also consistent with the observed increase in the CO stretching frequency by ~70 $cm^{-1}$ relative to the gas-phase value (more than that expected from simple mechanical coupling to the surface[22]) as the $5\sigma$ orbital is also weakly antibonding with respect to the CO bond.[73] These changes in CO electronic structure are relatively small, in agreement with the weak bonding interaction ($\Delta H_0$ = 12 kcal/mol). Moreover, these

(72) Brundle, C. R. In "Electronic States of Inorganic Compounds: New Experimental Techniques"; Day, P., Ed.; D. Reidel Publishing Co.: Boston, 1975; p 361.

(73) Snyder, L. C.; Basch, H. "Molecular Wave Functions and Properties"; Wiley: New York, 1972. Only the $3\sigma$ and $5\sigma$ contribute significantly to the C–O overlap with +0.6444 and −0.1461 populations, respectively.

electronic changes are what would be expected based on SCF-Xα-SW calculations of the bulk ZnO states,[74] noting that even in the bulk, the π overlap between the zinc $3d^{10}$ electrons, which are greatly stabilized because of the closed-shell configuration, and the oxide $2p_{x,y}$ orbitals is very small (only 8% of the electron density is on the oxides for the $5t_2$ state), whereas the σ interaction between the zinc 4s and 4p and the oxide $2p_z$ is much larger, particularly for the $6a_1$ state.

This geometric and electronic structure picture of CO on ZnO has implications concerning its reactivity, in particular with respect to the synthesis of methanol. The polarized molecule has a strengthened CO bond, initially making C–O bond rupture less probable, but making the molecule susceptible to heterolytic attack by dissociated $H_2$, which is known to adsorb as $Zn-H^-$ and $OH^+$.[75,76]

**Acknowledgment.** This research has been supported by the Department of Energy Contract Number ER-78-S-02-4988.A000 (R.R.G., M.H.N., and E.I.S.) and by the Department of the Air Force (V.E.H. and H.J.Z.), using equipment provided by the Department of the Air Force and supported by the Department of Energy. The authors are grateful to the following people for the gifts of ZnO single crystals: Dr. Charles Hurwitz, Dr. Klaus Fischer, Dr. Gunther Dierssen, Dr. Gary Rubloff, and Dr. Hans Lüth. We wish to thank the support staff at Lincoln Laboratory, particularly Mr. Bernie Feldman, for technical assistance, and Professor Read McFeely, Kevin D'Amico, and Michael Sayers (MIT) for continued interactions. The views and conclusions contained in this document are those of the contractor and should not be interpreted as necessarily representing the official policies, either expressed or implied, of the United States Government.

(74) Kowalski, J. M.; Johnson, K. H., unpublished results.
(75) Kokes, R. J. *Acc. Chem. Res.* **1973**, *6*, 226.
(76) D'Amico, K. L.; McClellan, M. R.; Sayers, M. J.; Gay, R. R.; McFeely, F. R.; Solomon, E. I. *J. Vac. Sci. Technol.*, in press.

# Studies of Energy-Transfer and Electron-Transfer Processes Involving the $^3A_{2u}$ Excited States of Binuclear Rhodium Isocyanide Complexes

**Steven J. Milder,[1a] Robert A. Goldbeck,[1b] David S. Kliger,[1b] and Harry B. Gray*[1a]**

*Contribution No. 6212 from the Arthur Amos Noyes Laboratory, California Institute of Technology, Pasadena, California 91125, and the Division of Natural Sciences, University of California, Santa Cruz, California 95064.* *Received April 21, 1980*

**Abstract:** The lowest electronic excited states of $Rh_2(br)_4^{2+}$ (br = 1,3-diisocyanopropane) and $Rh_2(TMB)_4^{2+}$ (TMB = 2,5-dimethyl-2,5-diisocyanohexane) are relatively long-lived emissive triplets ($^3A_{2u}$). The $^3A_{2u}$ lifetimes in acetonitrile are 8.5 ± 0.5 μs for $Rh_2(br)_4^{2+}$ and 25 ± 5 ns for $Rh_2(TMB)_4^{2+}$ (21 °C). The triplet energy of $Rh_2(br)_4^{2+}$ has been estimated to be about 39 kcal/mol (~1.7 eV, ~730 nm) from energy-transfer quenching experiments. The $^3A_{2u}$ excited states of $Rh_2(br)_4^{2+}$ and $Rh_2(TMB)_4^{2+}$ undergo electron-transfer reactions with oxidative and reductive quenchers. Reductive quenching by *N,N,N',N'*-tetramethyl-*p*-phenylenediamine (TMPD), and oxidative quenching by paraquat ($PQ^{2+}$) have been studied in detail. In methanol solution, $Rh_2(br)_4^{2+*}$ ($^3A_{2u}$) reacts with TMPD to give $Rh_2(br)_4^+$ and $TMPD^{+\cdot}$ ($k_b$, the back-reaction rate constant, is $1 \times 10^9$ $M^{-1}$ $s^{-1}$); similarly, $Rh_2(TMB)_4^{2+*}$ ($^3A_{2u}$) reacts with TMPD to give $Rh_2(TMB)_4^+$ and $TMPD^{+\cdot}$ ($k_b = 1.4 \times 10^9$ $M^{-1}$ $s^{-1}$). Oxidation of $Rh_2(TMB)_4^{2+*}$ ($^3A_{2u}$) by $PQ^{2+}$ in methanol gives $Rh_2(TMB)_4^{3+}$ and $PQ^{+\cdot}$ ($k_b = 2.2 \times 10^8$ $M^{-1}$ $s^{-1}$; $\mu = 1.95 \times 10^{-2}$ M). One-electron oxidation of $Rh_2(br)_4^{2+*}$ ($^3A_{2u}$) by $PQ^{2+}$ is observed, but the kinetics of the back-reaction are complex, owing to competing oligomerization processes.

## Introduction

For several years we have been investigating the photochemistry of polynuclear metal complexes.[2-8] Part of our work has centered on the reduction of protons to hydrogen by solar irradiation of polynuclear complexes in homogeneous solutions.[3-7] One discovery of note in this area is that 546-nm irradiation of $Rh_4(br)_8^{6+}$ (br = 1,3-diisocyanopropane) in concentrated hydrohalic acids results in clean conversion to $Rh_2(br)_4X_2^{2+}$ (X = Cl, Br) and $H_2$. Our studies of the mechanism of this photoreaction suggest that a cluster cleavage process ($Rh_4^{6+} + h\nu \rightarrow Rh_2^{4+} + Rh_2^{2+}$; $Rh_2^{2+} + H^+ + \Delta \rightarrow {}^1/_2Rh_4^{6+} + {}^1/_2H_2$) is involved.[7] Unfortunately, the quantum yields for the overall photoreaction are low.

Our recent work on the photochemistry of polynuclear rhodium isocyanides has taken a somewhat different direction. We have decided to explore the redox chemistry of the long-lived (8.5 μs in $CH_3CN$ solution)[8] triplet excited state ($^3A_{2u}$) of $Rh_2(br)_4^{2+}$. The photoredox chemistry of $Rh_2(br)_4^{2+}$ should be as rich as

(1) (a) California Institute of Technology. (b) University of California at Santa Cruz.
(2) (a) Geoffroy, G. L.; Gray, H. B.; Hammond, G. S. *J. Am. Chem. Soc.* **1974**, *96*, 5565. (b) Fleming, R. H.; Geoffroy, G. L.; Gray, H. B.; Gupta, A.; Hammond, G. S.; Kliger, D. S.; Miskowski, V. M. *Ibid.* **1976**, *98*, 48. (c) Erwin, D. K.; Geoffroy, G. L.; Gray, H. B.; Hammond, G. S.; Solomon, E. I.; Trogler, W. C.; Zagars, A. A. *Ibid.* **1977**, *99*, 3620. (d) Trogler, W. C.; Geoffroy, G. L.; Erwin, D. K.; Gray, H. B. *Ibid.* **1978**, *100*, 1160. (e) Trogler, W. C.; Gray, H. B. *Nouv. J. Chim.* **1977**, *1*, 475. (f) Trogler, W. C.; Gray, H. B. *Acc. Chem. Res.* **1978**, *11*, 232. (g) Miskowski, V. M.; Goldbeck, R. A.; Kliger, D. S.; Gray, H. B. *Inorg. Chem.* **1979**, *18*, 86. (h) Tyler, D. R.; Schmidt, M. A.; Gray, H. B. *J. Am. Chem. Soc.* **1979**, *101*, 2753. (i) Tyler, D. R.; Altobelli, M.; Gray, H. B. *Ibid.* **1980**, *102*, 3022.
(3) Mann, K. R.; Lewis, N. S.; Miskowski, V. M.; Erwin, D. K.; Hammond, G. S.; Gray, H. B. *J. Am. Chem. Soc.* **1977**, *99*, 5525.
(4) (a) Gray, H. B.; Mann, K. R.; Lewis, N. S.; Thich, J. A.; Richman, R. M. *Adv. Chem. Ser.* **1978**, *No. 168*, 44. (b) Mann, K. R.; Gray, H. B. *Ibid.* **1979**, *No. 173*, 225.
(5) Miskowski, V. M.; Sigal, I. S.; Mann, K. R.; Gray, H. B.; Milder, S. J.; Hammond, G. S.; Ryason, P. R. *J. Am. Chem. Soc.* **1979**, *101*, 4383.
(6) Gray, H. B.; Miskowski, V. M.; Milder, S. M.; Smith, T. P.; Maverick, A. W.; Buhr, J. D.; Gladfelter, W. L.; Sigal, I. S.; Mann, K. R. "Fundamental Research in Homogeneous Catalysis 3"; Tsutsui, M., Ed.; Plenum Press: New York, 1979, p 819.
(7) Sigal, I. S.; Mann, K. R.; Gray, H. B. *J. Am. Chem. Soc.*, in press.
(8) Miskowski, V. M.; Nobinger, G. L.; Kliger, D. S.; Hammond, G. S.; Lewis, N. S.; Mann, K. R.; Gray, H. B. *J. Am. Chem. Soc.* **1978**, *100*, 485.

0002-7863/80/1502-6761$01.00/0 